Egyptian Journal of Pure and Applied Science

Effective removal of cadmium ions from wastewater using modified mesoporous zeolite-A /reduced graphene oxide nanocomposite: kinetic and thermodynamic studies

Mohamed A. Farghali[1,2*], Mohamed M. Abo-Aly[3], Taher A. Salaheldin[4]

1 Nanotechnology and Advanced Materials Central Laboratory (NAMCL), Regional Center for Food and Feed (RCFF), Agricultural Research Center (ARC), Giza, Egypt.
2 Nanotechnology Research Centre (NTRC), British University in Egypt (BUE), Cairo, Egypt. 11837 - P.O. Box 43.
3 Chemistry Department, Faculty of Science, Ain Shams University, PO 11566 Cairo, Egypt.
4 Pharmaceutical Research Institute, Albany College of Pharmacy & Health Sciences, New York, USA. 12144.

ARTICLE INFO

Article history:
Received 6 August 2020
Accepted 1 october 2020

Keywords:
Mesoporous Zeolite-A/reduced graphene oxide;
Adsorption; Cadmium ions;
Langmuir isotherm;
pseudo second order.

ABSTRACT

This study discusses the capability of the prepared modified mesoporous zeolite-A /reduced graphene oxide nanocomposite (MZ-A/RGO) in removal of cadmium (Cd^{2+}) ions from wastewater, in which 3-aminopropyl- trimethoxysilane (APTMS) was used as a mesopore generating and cross linkage agent in this preparation. X-ray diffraction, attenuated total reflectance- Fourier transform infrared spectroscopy (ATR-FTIR) and field emission scanning electron microscope were used to confirm the successful preparation of MZ-A/RGO nanocomposite. The results indicated that the modified mesoporous zeolite-A (MZ-A) was attached to the surface of the reduced graphene oxide (RGO) nanosheets without any aggregation. The adsorption treatment experiments were conducted for Cd^{2+} ions removal and the adsorption capacities of MZ-A/RGO were determined under different adsorption parameters including, the contact time, initial adsorbate concentrations and temperature. The adsorption results revealed that 15 minutes was quiet enough to ensure the equilibrium state with maximum adsorption capacity 222.23 mg/g and the experimental data was fitted well with the pseudo-second-order kinetic model. The isotherm studies refer to the Langmuir model exhibits best fitting for the obtained experimental data and the thermodynamic results confirm that the endothermic nature of the adsorption of Cd^{2+} ions on MZ-A/RGO nanocomposite.

Introduction

Cadmium is one of the harmful heavy metals that are not essential for human bodies that have negative impacts to the human health and environment. In addition, its bioaccumulation and non-biodegradability nature in aqueous environments, continuous and long-term exposure of human to cadmium contaminates existing in food products and drinking water could be led to severe damage for kidney, liver, pancreas, lung function, or produce cardiovascular diseases and erythrocyte destruction, nausea, diarrhea, hypertension, muscular cramps, skeletal deformities and chronic pulmonary problems [1-3].

WHO organization and the US Environmental Protection Agency (USAEPA) stated that the maximum concentration level of cadmium contaminant in drinking water is 0.003 and 0.005 mg/L, respectively [4]. To meet these water quality criteria different wastewater treatment techniques was applied such as chemical precipitation, flocculation, coagulation, membrane filtration, ion exchange, reverse osmosis and adsorption. Adsorption is most common and convenient technique in wastewater treatment due to its high removal efficiency, cost-effectiveness, ease of operation, adsorbent recycling and the feasibility of applying it on a large scale [5-8].

Graphene nanosheet is widely used as a nanoadsorbent in treatment of different types of contaminants, such as organic and inorganic contaminants [9, 10]. Nevertheless, the efficiency of graphene is limited due to the tendency of the graphene to aggregate that lead to lowering of its surface area and decreasing its adsorption capacity. In addition, it is difficult to separate graphene from aqueous solution after adsorption process take place.

* Corresponding author.
E-mail address: mgoda199@gmail.com

This limitation could be overcome by applying surface modification of graphene such as attaching another nanoadsorbent on the surface of graphene nanosheets which enhance the adsorption capacity of the graphene based nanocomposite [11, 12].

Zeolites are aluminosilicate minerals with a surface structure containing a great number of electrostatic holes that are occupied by cations and water molecules. The uptake in zeolites occurs through the movement of the cations and water molecules allowing the ion exchange mechanism and reversible dehydration process. Numerous types of zeolite have been known and effectively used in the uptake of heavy metals from wastewater [13]. one of these types is zeolite-A or NaA zeolites that is widely used in water treatment with pore diameter of 4–5 Å. Sodium cations are located in the alpha cage of zeolite-A structure which are responsible for ion exchange. Exchange of Si by Al produce charge imbalance to zeolite and decreasing in Si/Al molar ratio that causes increasing the negativity in zeolite structure and increasing the cation exchange capacity which make it effective in removal of the heavy metal ions [14]. In order to further increase the adsorption capacity of MZ-A, attaching of zeolite-A on RGO could enhance the adsorption capacity of MZ-A/RGO nanocomposite for heavy metals [15].

Therefore, the objective of this study is to maximize the removal efficiency for Cd^{2+} ions based on preparation of MZ-A/RGO nanocomposite, in which APTMS was used as a mesopore generating and cross linkage agent in this preparation using hydrothermal synthesis method. The physicochemical properties of the prepared nanocomposites were confirmed by a set of characterization techniques. The adsorption kinetic, isotherm and thermodynamic studies of the MZ-A/RGO nanocomposite for Cd^{2+} ions were investigated.

Material and methods

Subjects

High purity chemicals were purchased from Sigma-Aldrich and otherwise was stated, all chemicals were used without additional purification, graphite powder with average particle size < 20 μm, sulfuric acid (97 wt. %), hydrochloric acid (37 wt. %, ACS reagent), sodium nitrate (99.5 wt. %), potassium permanganate (99.0 wt. %), sodium hydroxide pellets (≥ 97.0 wt. %, ACS reagent), hydrogen peroxide (32 wt. %, Alfa Aesar), sodium silicate solution, sodium aluminate anhydrous, ethanol (HPLC grade, Fisher), propanol (> 99.5 wt. %, Alfa Aesar), 3-aminopropyl trimethoxysilane solution (APTMS, 97.0 wt.%) and cadmium chloride dihydrate (99.0 wt. %).

Adsorbents preparation

Preparation of zeolite-A

In this study sodium aluminate and sodium silicate reagents were used as Al and Si sources in the preparation of zeolite-A [16]. The molar ratios of the starting materials were 1 Al_2O_3: 3.4 SiO_2: 0.8 NaOH: 370 H_2O: 19.6 C_2H_5OH: 6 C_3H_7OH, the raw materials were vigorously mixed using magnetic stirrer at room temperature, then, the reaction mixture was treated hydrothermally in 100 mL teflon-lined stainless-steel autoclaves and heated in oven for 24 h at 110 °C. The resulted product was filtered and washed several times using DI water until the solution pH less than 9.0. Thereafter, the white precipitate was dried in oven at 100 °C.

Preparation of the modified mesoporous zeolite-A/ reduced graphene oxide (MZ-A/RGO) nanocomposite

The preparation of MZ-A/RGO was performed into two steps, as a follow: First step, including the preparation of GO which occurs according to our previous study [17] using modified Hummers method. Second step, MZ-AG is prepared according to [18] with modification. In which 0.5 g of zeolite-A powder was add to 100 mL of ethanol solution. The mixture was sonicated and stirred for 1 h at room temperature, followed by addition of 2 mL of APTMS solution to the mixture with continuous stirring at room temperature for 30 min. Subsequently, the preparation of MZ-A/RGO is performed by addition of 0.5 g of the prepared GO into the above mixture at room temperature with stirring for 2 h. then, the total mixture was transferred to Teflon-lined stainless-steel autoclave for 24 h at 170 °C for hydrothermal treatment. Thereafter, the precipitate was collected by centrifugation at room temperature for 10 min and washed several times with ethanol, followed by drying in an oven at 70 °C.

Materials characterization

The physicochemical characterization of the prepared nanomaterials and nanocomposite were performed using powder X-ray diffractometer (XRD, X'Pert PRO PANalytical, Netherlands) equipped with a CuKα radiation source (λ=1.5404 Å) to determine the crystal structure of the materials, Fourier transform infrared spectroscopy equipped with the attenuated total reflectance-ATR diamond crystal unit (ATR-FTIR, VERTEX 70 RAM II-ATR, BRUKER, Germany) used to identify the functional groups of the prepared materials, Field emission scanning electron microscope (FESEM, Quattro S, Thermo Scientific, USA) was used for the purpose of imaging, studying the surface morphology and size of the prepared nanomaterials.

Batch adsorption experiments

Batch adsorption studies including different parameters such as, contact time, initial adsorbate concentrations and temperature were changed to examine the adsorption capacity and removal efficiency of MZ-A/RGO and MZ-A for Cd^{2+} ions. Furthermore, the adsorption kinetics, isotherms and thermodynamic were studied, in which certain volume (100 mL) containing known concentration of Cd^{2+} ions aqueous solution (10 – 500 mg/L) was shaken on a bench top shaker (Heidolph Unimax 1010, Germany) at 300 rpm after addition of a known weight of sorbents (0.05 g) at specific time intervals from 0 – 120 min, small portion from the aqueous solution was withdrawn and instantly filtered using 0.22 μm syringe filters. The remaining Cd^{2+} ions concentration after completing the adsorption process was determined by inductively coupled plasma optical emission spectrometry (ICP–OES; Avio 500, PerkinElmer, USA). The equilibrium adsorption capacity (q_e, mg/g) and removal efficiency (%) of MZ-A/RGO and MZ-A for Cd^{2+} ions adsorption was calculated by the following equations, respectively [19].

$$q_e = \left(\frac{C_o - C_t}{M}\right) V \quad (1)$$

$$R\% = \left(\frac{C_o - C_t}{C_o}\right) * 100 \quad (2)$$

Where C_o and C_t are the concentration of Cd^{2+} ions (mg/L) in aqueous solution before and after adsorption process, respectively. V (L) is the solution volume, M (g) is the weight of the adsorbent added and q_e (mg/g) is the sorption capacity of the adsorbent, which is terms to the equilibrium amount of Cd^{2+} ions (adsorbate) adsorbed per gram of sorbent.

Adsorption kinetics study

The contact time is an important factor which explains the kinetics of the adsorption process and control the capability of an adsorbent for practical usage and its influences on the economic efficiency of the adsorption process [20]. In order to investigate the kinetics of adsorption process, pseudo-first order, pseudo-second order and Elovich kinetic models were applied [21]. The pseudo-first-order model is assumed that the adsorption rate is controlled by chemical adsorption, which includes the electron transfer and sharing between adsorbent and adsorbate. The pseudo-first-order is generally described by the following equation [22].

$$\ln(q_e - q_t) = \ln q_e - K_1 t \quad (3)$$

Where q_t and q_e are the adsorption capacities (mg/g) at specific time t (min) and at equilibrium, respectively; K_1 (min^{-1}) is the pseudo-first-order rate constant. The values of K_1 and $\ln q_e$ can be obtained from the slope and intercept of linear plotting of $\ln (q_e - q_t)$ vs. t, respectively.

The pseudo-second-order model supposes that the interaction between the adsorbate and adsorbent occurs through their valence forces. The pseudo-second-order is expressed by the following equation [23].

$$\frac{t}{q_t} = \frac{1}{K_2 q_e^2} + \left(\frac{1}{q_e}\right) t \quad (4)$$

Where K_2 (g/mg·min) is the second-order adsorption rate constant. The values of q_e and K_2 can be obtained from the slope and intercept of the linear plot of t/qt vs. t, respectively. Furthermore, the term h (mg/g.min) represented the initial sorption rate:

$$h = K_2 q_e^2 \quad (5)$$

Elovich kinetic model adequate for adsorption in heterogeneous surfaces influenced by diffusion factor and reaction rate together. Elovich kinetic model is given by the following equation [24].

$$q_e = \left(\frac{1}{\beta}\right) \ln(\alpha\beta) + \left(\frac{1}{\beta}\right) \ln t \quad (6)$$

Where α is the initial adsorption rate (mg/g·min) and β is the desorption constant related to the extent of surface coverage and activation energy for chemisorption (g/mg). The Elovich constants (α, β) can be obtained from the plotting q_t vs. $ln\ t$, which yields a straight line with a slope and intercept equal to ($1/\beta$) and ($1/\beta$)ln($\alpha\beta$), respectively [22].

Adsorption isotherms study

Adsorption isotherm mechanisms illustrates the interaction behavior between adsorbent and adsorbate and adsorbate contaminants [25]. To determine the adsorption isotherms mechanism, Langmuir, Freundlich, Temkin, and Dubinin–Radushkevich (D–R) models were employed [21, 26]. Langmuir isotherm is an empirical model supposing that monolayer adsorption take place on the surface of adsorbent in which adsorption process occurs at identical and equivalent fixed sites and finite number of adsorption sites on the adsorbent surface is available and only one adsrobate particle can be adsorbed at each adsorption site and there is no steric hindrance and interaction between the adsorbed molecules even on adjacent sites [27]. Furthermore, homogenous adsorption takes place in which each molecule possesses its sorption activation energy and constant enthalpies independently. In addition, all sites have equal affinity towards the adsorbate molecules, and no adsorbate migration occurs in the surface plane. The linear mathematical equation of the Langmuir isotherm model represented as [28].

$$\frac{C_e}{q_e} = \frac{1}{b q_{max}} + \left(\frac{1}{q_{max}}\right) C_e \quad (7)$$

Furthermore, separation factor (R_L) is a dimensionless constant which is defined as:

$$R_L = \frac{1}{1 + b\, C_o} \quad (8)$$

Where, $C_{o_\circ}$ is the initial adsorbate concentration (mg/L) and b is Langmuir constant which is related to the adsorption capacity in (mg/g). Depending on the values of the separation factor (R_L), the nature of the adsorption process is determined. In which the adsorption is linear if $R_L = 1$, irreversible if $R_L = 0$, unfavorable if $R_L > 1$, or favorable if $0 < R_L < 1$ [29].

Freundlich adsorption isotherm model describe the adsorption process on a heterogeneous surface and it is applied for the reversible and non-homogenous adsorption process. Freundlich model is not limited to the monolayer adsorption, it is valid also to describe the multilayer adsorption process. In this isotherm model, adsorption affinities and heat does not necessity to be equally distributed on the heterogeneous surfaces. Freundlich isotherm model is applicable to define the heterogeneity of the surface and the exponential distribution of the active site's energies. Freundlich model is described by the following equation [25].

$$\ln q_e = \ln k_f + \left(\frac{1}{n}\right) \ln C_e \quad (8)$$

where C_e and q_e are the adsorbate concentration (mg/L) and adsorption capacity (mg/g) at equilibrium, respectively and k_f and n are the Freundlich isotherm constants, which are temperature dependent [30]. The values of n and k_f can be obtained from the slope and intercept, respectively, of a plot of $ln\ q_e$ against $ln\ C_e$. the $1/n$ is the intensity of the adsorption or surface heterogeneity indicating the energy relative distribution and the heterogeneity of the adsorbate sites. The adsorption process is unfavorable when $1/n > 1$, favorable when $0 < 1/n < 1$ and it is irreversible when $1/n = 1$ [25].

Temkin is an empirical isotherm model takes into account the interaction between the adsorbent and the adsorbate in which it disregards the extremely low and large concentration values. This model supposes that heat of adsorption (ΔH_{ads}) as a function of temperature decrease linearly rather than logarithmically for all molecules existing on the surface layer because the surface coverage increases. This adsorption isotherm model is only applied for an intermediate concentration range. Otherwise, this model is not suitable to describe complex adsorption systems including aqueous-phase adsorption isotherms. The linear form of the Temkin model is described by the following equation [25, 31].

$$q_e = B \ln A_T + B \ln C_e \quad (9)$$

where C_e and q_e are the adsorbate concentration (mg/L) and sorption capacity (mg/g) at equilibrium, respectively. B is equal to (RT/b_T), b_T is the Temkin constant related to the heat of adsorption (ΔH_{ads}) in (J/mol), R is the universal gas constant (8.314 J/mol·K), T is the absolute temperature (298 K), and A_T is the Temkin isotherm equilibrium binding constant (L/g) corresponding to the maximum binding energy. The values of b_T and A_T can be obtained from the slope and intercept by plotting q_e vs. $ln(C_e)$, respectively [32].

Dubinin-Radushkevich (D-R) adsorption isotherm model is used to describe the adsorption mechanism onto the heterogeneous surfaces using the Gaussian energy distribution and it is temperature dependent. D-R model is a semiempirical equation in which the adsorption pursues the mechanism of pore filling. It is used to describe a multilayer adsorption and it is suitable for the physical adsorption processes with Van der Waal's interaction forces. This isotherm model ordinarily is to differentiate between the physical and chemical adsorption mechanisms depending on the mean free energy. D-R model has the following linear form equations [25, 31].

$$\ln q_e = \ln(q_{th}) - (K_{DR}\varepsilon^2) \quad (10)$$

Where q_e and q_{th} are the sorption capacities at equilibrium and theoretical isotherm saturation capacity (mg/g), respectively; K_{DR} (mol^2·K/J^2) is the D–R isotherm constant related to adsorption energy and ε is the Polanyi energy. The constants K_{DR} and q_{th} can be obtained from the slope and intercept, respectively of the plotting $ln\ q_e$ vs. ε^2

The Polanyi energy ε can be calculated using Equation 11:

$$\varepsilon = RT \ln\left(1 + \frac{1}{C_e}\right) \quad (11)$$

Where C_e is the adsorbate concentration at equilibrium (mg/L), R is the universal gas constant (8.314 J/mol·K), and T is the absolute temperature (K).

Adsorption thermodynamics study

The sorption process is temperature dependent, so adsorption experiments were performed at various temperatures. MZ-A/RGO (0.05 g) was added to a solution of Cd^{+2} ions (200 mg/L, 100 mL) at four different temperatures (298, 313, 333, and 353 K).

The thermodynamic parameters, such as the Gibbs free energy change (ΔG^o), can be calculated using Equation 12:

$$\Delta G^o = -RT \ln K_d \quad (12)$$

Where K_d is the thermodynamic Langmuir constant for the adsorption process [L/mg], calculated using Equation 13:

$$K_d = \frac{q_e}{C_e} \quad (13)$$

The entropy ($\Delta S°$) and enthalpy ($\Delta H°$) parameters were determined from the intercepts and slope of the linear plotting between $ln\ K_d$ vs. $1/T$ according to Equation 14:

$$\ln K_d = \frac{\Delta S^o}{R} - \frac{\Delta H^o}{RT} \quad (14)$$

Results and discussion

Characterization of the prepared nanosorbents

XRD patterns for the GO, zeolite-A and MZ-A/RGO nanocomposite are shown in **Fig. 1**. The XRD of GO exhibited significant peak at 2θ=11.0° suggesting the successful oxidation and transformation of graphite to GO using modified Hummers method. XRD pattern of zeolite-A exhibited characteristic diffraction peaks of zeolite-A at 2θ=7.16°, 10.16°, 12.44°, 21.65°, 24.01°, 26.28°, 27.12°, 29.92°, and 34.18° that congruent with zeolite-A (Na) JCPDS reference card (01-073-2340) of the cubic structure with the chemical formula $Na_{12}Al_{12}Si_{12}O_{48}{\cdot}27H_2O$, indicating the successful preparation of pure phase of zeolite-A [15]. on the other hand the XRD pattern of MZ-A/RGO nanocomposite is very close to the pattern of zeolite-A without any considerable shift in peak positions of zeolite-A, indicating that APTMS has no influence on the internal chemical structure of zeolite-A [33]. in addition to, the very broad and weak peak around 2θ=24.0° is attributed the successful reduction of GO to RGO and the spacing between planes is decreased from 0.80 nm of the (001) reflection plane in case of GO to 0.37 nm of the (002) reflection plane in case of RGO, suggesting the reduction of the oxygen related functional groups of GO in the presence of amino groups of the used APTMS through the hydrothermal treatment and formation of RGO [15]. The presence of RGO in the nanocomposite does not affect the crystallinity of zeolite-A, but only affect the intensity of the MZ-A/RGO nanocomposite peaks indicating the successful overlapping between the zeolite-A and RGO and fabrication of MZ-A/RGO nanocomposite in presence of APTMS as crosslinking material in the preparation process of the nanocomposite [34].

The ATR-FTIR curve of the GO, zeolite-A and MZ-A/RGO nanocomposite was displayed in **Fig. 2**, GO exhibited a set of bands at 1046 cm^{-1}, 1226 cm^{-1}, 1405 cm^{-1}, 1616 cm^{-1}, 1720 cm^{-1} and 3300 cm^{-1}, assigning to alkoxy C–O stretching vibrations, epoxy C–O stretching vibrations, carboxyl O=C–O stretching vibrations, sp^2-hybridized C=C vibrations, C=O stretching vibrations and –OH stretching vibrations in water molecules, respectively. That confirm the attaching of various oxygen containing functional groups on the GO surface [35, 36].

The spectrum of zeolite-A displays the characteristic absorption band for the zeolite structure Si–O and Al–O at 995 cm^{-1} and the peaks at 468, 547 and 663 cm^{-1} are attributed to the crystallinity of zeolite-A. the broad absorption band at 3364 cm^{-1} are assign to –OH stretching vibrations of the absorbed water in the zeolite structure [37-39].

On the other hand, The ATR-FTIR spectrum of MZ-A/RGO nanocomposite displays either the evanescence of the absorption bands at 1046, 1405 and 1720 cm^{-1} or a major decrease in intensity at 1226 and 3300 cm^{-1} of the most predominant oxygen functional groups on GO surface, which confirmed the reduction of GO and formation of RGO [40]. In addition to, the absorption bands existing at 468, 553, 673 and 1010 cm^{-1} suggesting the presence of zeolite-A structure with small displacement from the pure zeolite-A. The absorption bands located at 793 and 1047 cm^{-1} is attributed to the stretching vibration mode in Si–O–Si and asymmetric stretching in Si–O–Si, respectively, indicating the successful attaching of APTMS on the surface of zeolite-A and formation of MZ-A [41]. The broad absorption band existing at 3300 cm^{-1} is sharing between the –OH stretching vibrations band of water molecules and the N-H stretching vibration band of the APTMS attached to the negatively charged RGO surface. So, in the absence of added external reducing agents, the amino groups of the used APTMS was believed to be responsible for the in-situ reduction of GO to RGO through the hydrothermal treatment, suggesting the successful modification of the zeolite-A and RGO surfaces with APTMS through the silylation reaction [42, 43].

The surface morphology and imaging of the prepared nanomaterials are observed using scanning electron microscopy (SEM) as shown in **Fig. 3**. SEM of GO **Fig. 3a**, exhibited wrinkled and rough surface [44]. **Fig. 3b**, exhibited the surface imaging of MZ-A with the cubic like crystal structure of zeolite-A with average particle size of 1 µm, the image indicated the presence of surface agglomeration which decrease the total surface area of the prepared MZ-A [45]. In addition, it is obviously shown the presence of pores on the surface of the MZ-A due to the attaching of APTMS on the surface of MZ-A and formation of mesopores zeolite-A structure, in which APTMS acting as a mesopore generating agent. On the other hand, the great overlap and homogeneity between MZ-A and RGO is evident in the SEM of the MZ-A/RGO nanocomposite as indicated in **Fig. 3c**, suggesting the role of APTMS as cross linkage agent in the interaction between MZ-A and RGO and formation of MZ-A/RGO nanocomposite with no agglomeration between MZ-A particles.

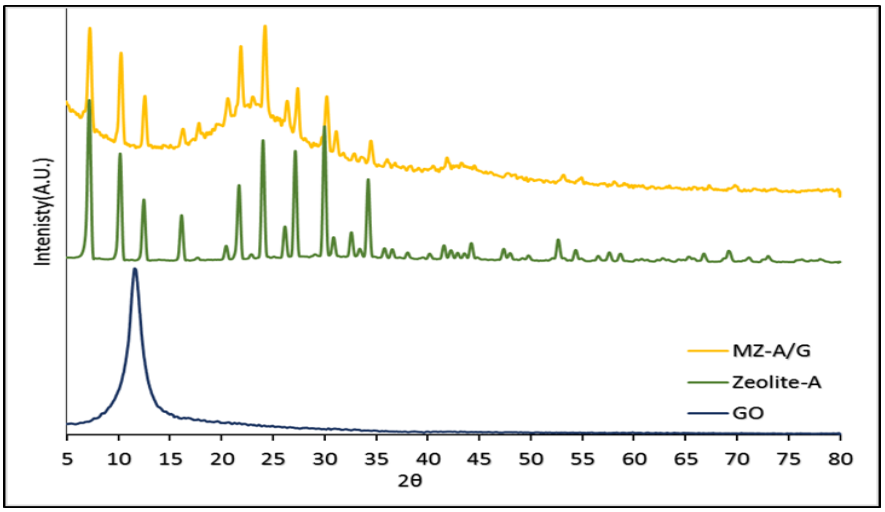

Fig. 1: XRD patterns of GO, MZ-A and MZ-A/RGO nanocomposite.

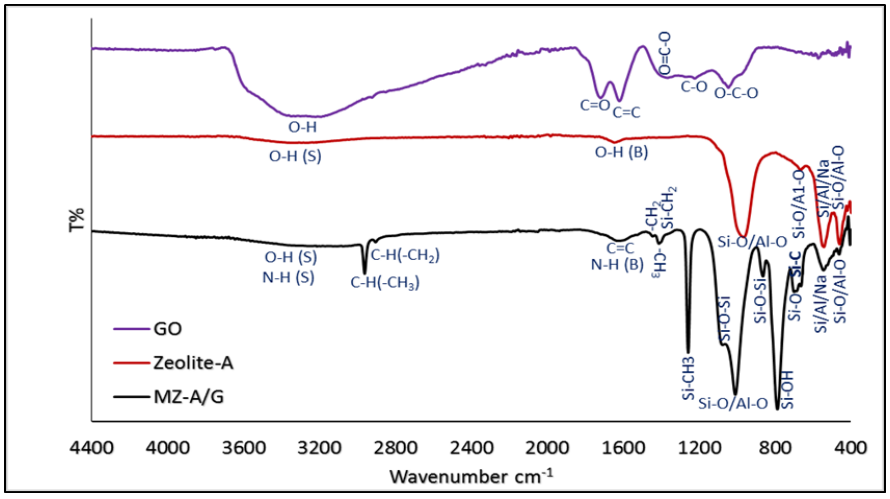

Fig. 2: ATR-FTIR spectra of GO, MZ-A and MZ-A/RGO nanocomposite.

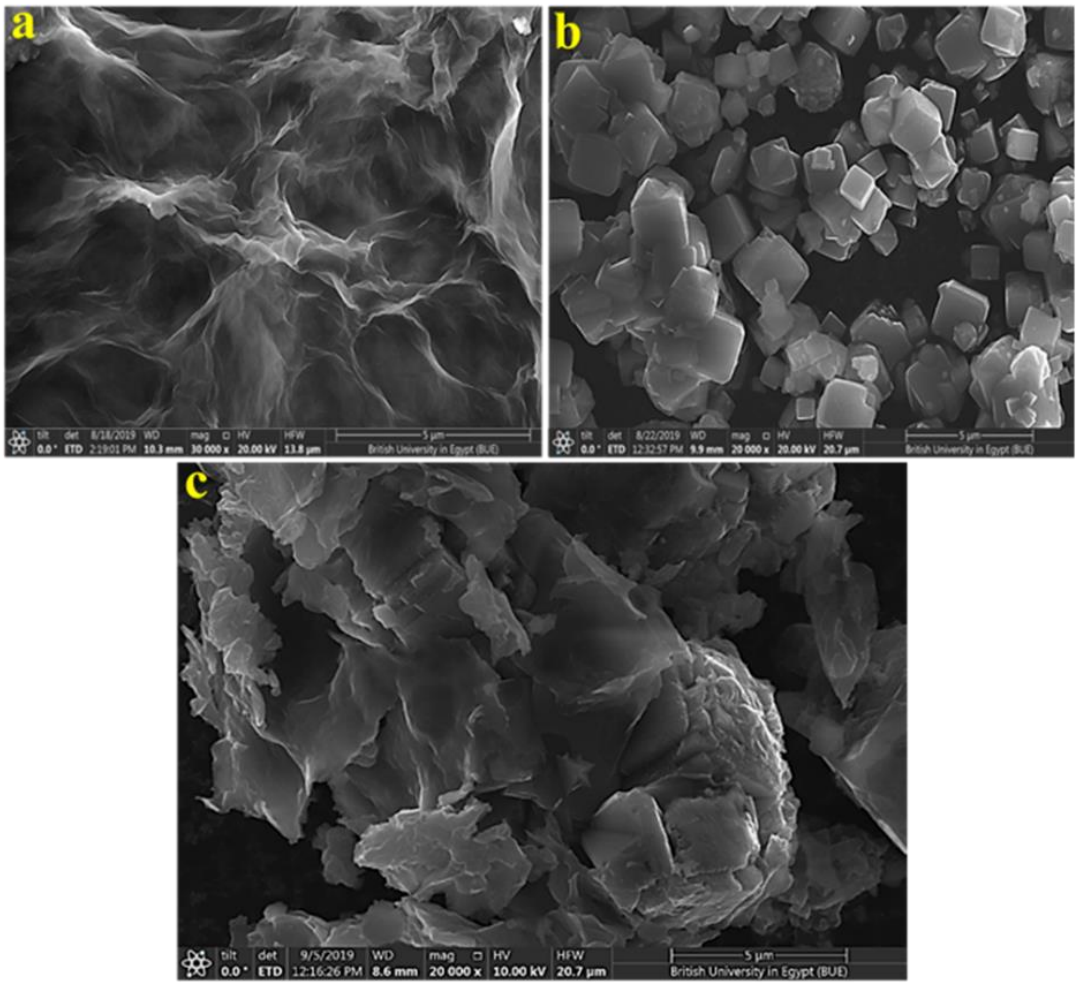

Fig. 3: SEM images for (a) GO, (b) MZ-A and (c) MZ-A/RGO nanocomposite.

Adsorption study

Effect of contact time and adsorption kinetics study

The comparative study of Cd^{2+} ions adsorption using MZ-A/RGO and MZ-A was displayed in **Fig. 4a**. It is clearly observed that the adsorption capacity of MZ-A/RGO nanocomposite was much higher than in case of MZ-A for removal of Cd^{2+} ions due to agglomeration of the MZ-A particles that causes decrease in the active sites and adsorption capacity of MZ-A. Furthermore, the removal of Cd^{2+} ions was very fast during the first 15 min. (q_e, Cd^{2+}=150 and 71.2 mg/g for MZ-A/RGO and MZ-A, respectively). After that, the adsorption capacity increases slowly until the adsorption equilibrium is reached at 162 mg/g for MZ-A/RGO and 98.6 mg/g for MZ-A after 120 min. This can be attributed to the availability of large numbers of active sites on the surface of MZ-A/RGO for Cd^{2+} ions to be adsorbed in the first stage of the adsorption process. In which, at the beginning very high adsorption driving forces lead to a higher adsorption capacity. However, after the first 15 min, slower adsorption may be attributed to the slower diffusion of Cd^{2+} ions into the interior pores of the zeolite. Also, the Cd^{2+} ions subsequently occupy the exchangeable positions within the crystal framework [46].

Several kinetics models have been discussed to evaluate the experimental data and to clarify the adsorption process of MZ-A/RGO and MZ-A. The kinetic data of the adsorption of Cd^{2+} ions was investigated using pseudo-first-order, pseudo-second-order and Elovich kinetic models **Fig. 4b-4d**. As can be seen, the correlation coefficients (R^2) of the pseudo-second-order model are more acceptable in comparison to the pseudo-first-order and Elovich models. Furthermore, the calculated q_e values of MZ-A/RGO and MZ-A for Cd^{2+} ions adsorption was 163.9 and 104.16 mg/g, respectively, obtained from the pseudo-second-order shows a better conformity with the q_e values obtained from the experimental data 162.0 and 98.6 mg/g. Also, the kinetic parameters for each model were calculated and are listed in **Table 1**. In addition to, these results indicates that the adsorption of Cd^{2+} ions on MZ-A/RGO and MZ-A obeys the pseudo-second-order model which depend on the hypothesis that adsorption may be the rate limiting step involving valence forces through exchange or sharing of electrons between adsorbate and adsorbent [47].

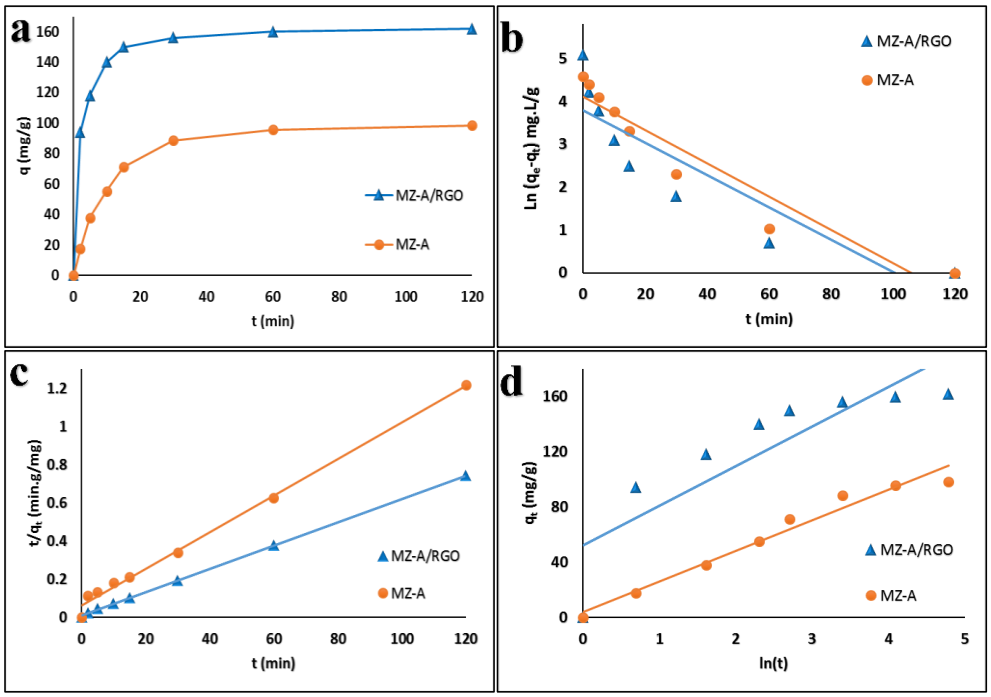

Fig. 4: Adsorption kinetics studies. (a) Effect of contact time on the adsorption capacity of MZ-A/RGO nanocomposite and MZ-A for Cd^{2+} ions and Fitting of the obtained kinetic results using (b) the pseudo-first-order equation (c) the pseudo-second-order equation and (d) the Elovich kinetic model.

Table 1: Kinetics parameters and constants for the adsorption of Cd^{2+} ions by MZ-A/RGO nanocomposite and MZ-A.

Adsorbent	*Pseudo-first-order model*			*Elovich model*		
	q_{Calc} *[mg/g]*	K_1 *[min^{-1}]*	R^2	*β [g/mg]*	*α [mg/g.min]*	R^2
MZ-A/RGO	43.91	0.038	0.786	0.0348	176.59	0.745
MZ-A	61.06	0.039	0.913	0.0452	26.41	0.9696
Adsorbate	**Pseudo-second-order model**					
	K_2 *[g/mg.min]*	q_{Calc} *[mg/g]*	q_{Exp} *[mg/g]*	*h [mg/g.min]*	R^2	
MZ-A/RGO	0.0047	163.93	162.0	125.0	0.9998	
MZ-A	0.0015	104.17	98.6	16.03	0.9995	

Effect of initial concentration and adsorption isotherms study

Adsorption isotherms are used to describe the interaction between the metal ions and the sorbent that play a necessary role in the determination of the maximum equilibrium adsorption capacity. Adsorption isotherms also used to evaluate of the economic viability of different sorbents for the commercial success [48]. The adsorption capacity of MZ-A/RGO for Cd^{2+} ions with different initial concentrations was shown in **Fig.5a**, the results indicates that the as the initial concentration increased from 10 to 500 mg/L the adsorption capacities increased from 19.9 to 218 mg/g. This is due to, at low concentrations of Cd^{2+} ions the ratio between Cd^{2+} ions species and the number of available active sites of the sorbent for adsorption is small, leading to mass transfer resistance between the sorbent and the adsorbate aqueous solution and thus decreasing the adsorption capacity [49]. Contrariwise, additional driving force that is exceed the mass transfer resistance of metal ions produced with increasing of the initial concentration of Cd^{2+} ions species, leading to an increase in adsorption capacity [5]. Different adsorption isotherms such as Freundlich, Langmuir, Temkin and Dubinin–Radushkevich (D-R) models were used to investigate the reaction mechanism as shown in **Fig. 5b-5e** and the fitted adsorption isotherm parameters based on the experimental data obtained for the adsorption of Cd^{2+} ions on MZ-A/RGO are summarized in **Table 2**. The results indicate that the correlation coefficient R^2 of Langmuir for Cd^{2+} ions adsorption was higher than for the other Freundlich, Temkin and Dubinin–Radushkevich (D-R) models. The ordering of R^2 is Langmuir> Temkin> Freundlich> D–R isotherm. So, the experimental data of adsorption were fitted well to the Langmuir model. Therefore, the coverage of Cd^{2+} ions examined on the surface of the MZ-A/RGO may be defined as a monolayer [50]. Furthermore, the values of the q_{max} and b for Cd^{2+} ions are 222.23 and 0.043, respectively. Suggesting the presence of a Van der Waals adsorption [51]. in addition, the separation factor (R_L) value which decide the favorability of the adsorption process: R_L >1 refers to unfavorable adsorption, R_L=1 refers to linear adsorption, 0 < R_L < 1 refers to favorable adsorption, and R_L=0 refers to irreversible adsorption, in this case, the values of the separation factor (R_L) for Cd^{2+} ions was in the range of 0 < R_L < 1 indicating the favorability of the adsorption process on the surface of MZ-A/RGO [52, 53]. Also, the values of experimental and theoretical maximum adsorption capacity (q_m) are much close to each other, indicating the good fitting of the Langmuir model. Comparison of maximum adsorption capacity (q_m) of MZ-A/RGO nanocomposite adsorbent with other reported different adsorbents for Cd^{2+} ions are listed in **Table 3**.

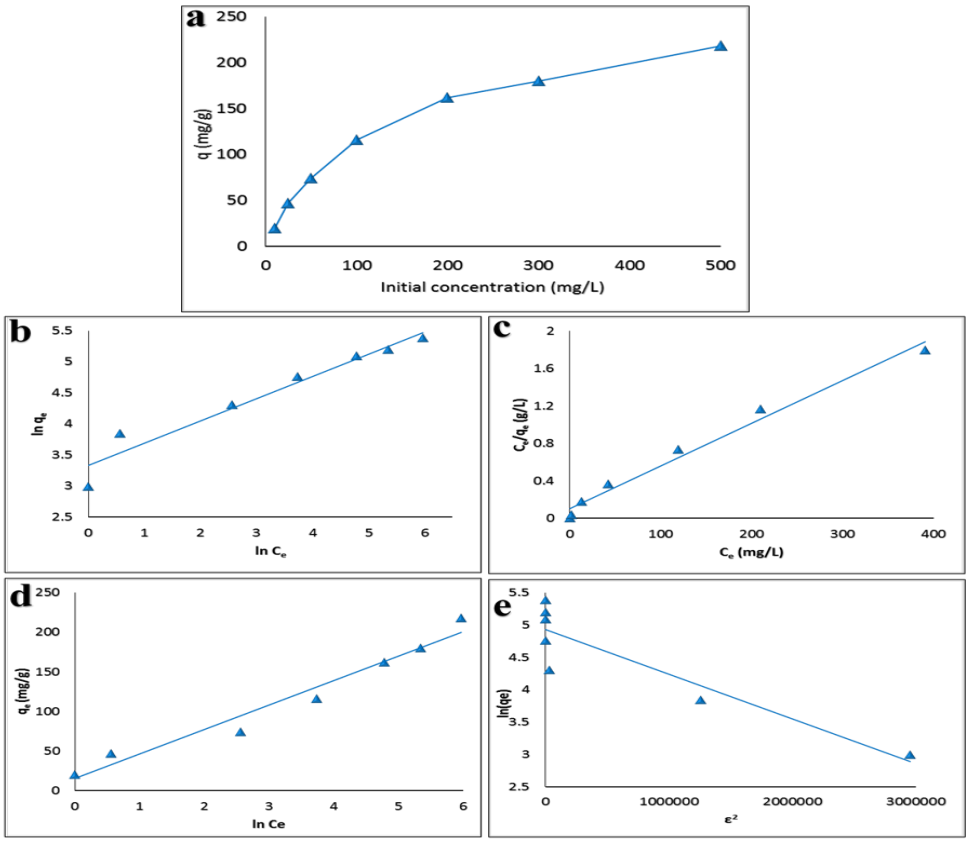

Fig. 5: Adsorption isotherms studies. (a) Initial concentration effect of Cd^{2+} ions on MZ-A/RGO nanocomposite and fitting of the obtained isotherm results using (b) Freundlich isotherm model, (c) Langmuir isotherm model, (d) Temkin isotherm model and (e) Dubinin–Radushkevich (D–R) isotherm model.

Table 2: Isotherm parameters, constants and correlation coefficients for the adsorption of Cd^{2+} ions on MZ-A/RGO nanocomposite using different isotherm models

Isotherm models	Kinetics parameters			
Freundlich isotherm	1/n		K_f (mg/g)	R^2
	0.358		27.99	0.947
Langmuir isotherm	q_{max} (mg/g)	b (L/mg)	R_L	R^2
	222.23	0.043	0.70–0.045	0.982
Temkin isotherm	B	b_T (J/mol)	A_T (L/g)	R^2
	30.95	80.05	0.99	0.963
D–R isotherm	q_{max} (mg/g)		K_{DR} ($mol^2.K/J^2$)	R^2
	137.80		$7x10^{-7}$	0.830

Table 3: Comparison of the maximum adsorption capacities of Cd^{2+} ions in this study with previous work at room temperature.

Adsorbent	Adsorption capacity, q_e [mg/g]	Reference
Zeolite Molecular Sieve	182.6	[54]
Zeolite-A	149.0	[55]
Polyacrylic acid-based hydrogel	169.70	[56]
Graphene oxide (GO)	139.9	[57]
Zeolite-supported microscale zero-valent iron (Z-mZVI)	63.14	[58]
Composite chitosan biosorbent	108.7	[59]
PS-GO gel	136.98	[60]
Magnetic p(AMPS) composite hydrogels	140.85	[61]
Coral strands	189	[62]
β-cyclodextrin/graphene oxide	196.07	[63]
magnetic biochar composites	46.90	[64]
Graphene aerogels	149.25	[5]
MnO2/o-MWCNTs)	41.60	[65]
MZ-A/RGO	**222.23**	**This work**

Effect of temperature and thermodynamic analysis

Adsorption capacity of MZ-A/RGO for Cd^{2+} ions was investigated at different temperatures and the corresponding plots were shown in **Fig. 6a**. the thermodynamic parameters of the adsorption process was calculated and reported in **Table 4**. The $\Delta H°$ and $\Delta S°$ were calculated from the slope and intercept of the plot of $ln\ K_d$ against $1/T$, **Fig. 6b**, and the values of $\Delta G°$ at different temperatures were calculated from equation (12). The value of $\Delta H°$ is very valuable for predicting the type of adsorption. Physisorption is generally below 20 kJ/mol and in the range 20–80 kJ/mol the physisorption together with chemisorption takes place and in the range 80–400 kJ/mol chemisorption occurs [66]. According to table (4) the value of $\Delta H°$ for Cd^{2+} ions is 5.67 kJ/mol. This indicates a physical adsorption process occurs. In addition to, the positive value of $\Delta H°$ for the adsorption process of Cd^{2+} ions on MZ-A/RGO shows that the adsorption was an endothermic process with random characteristics. The negative values for $\Delta G°$ at all temperatures indicate the spontaneously of the adsorption process. Furthermore, the values of $\Delta G°$ decrease as the temperature increase suggests that the adsorption process is more favorable at higher temperatures [67]. Furthermore, the positive value of the entropy change $\Delta S°$ is 21.5 J/mol.K,indicating an increase in randomness at the solid/solution interface during the adsorption process [68].

Conclusion

The objective of this work is to enhance the attaching of the mesoporous zeolite-A on the surface of the RGO through the hydrothermal treatment by using APTMS as a mesopore generating and binding agent and formation of MZ-A/RGO nanocomposite, the presence of the mesoporous zeolite-A on the surface of the RGO decrease the agglomeration of the MZ-A and RGO that could enhance the removal efficiency of Cd^{2+} ions onto MZ-A/RGO under different adsorption conditions such as contact time, initial Cd^{2+} ions concentration and temperature. The fabricated MZ-A/RGO nanocomposite was characterized by different analytical techniques to prove the successful of the preparation method. The pseudo-second-order kinetic model and the Langmuir adsorption isotherm equation exhibited better fitting for the adsorption of Cd^{2+} ions onto MZ-A/RGO based on the values of the correlation coefficients (R^2).

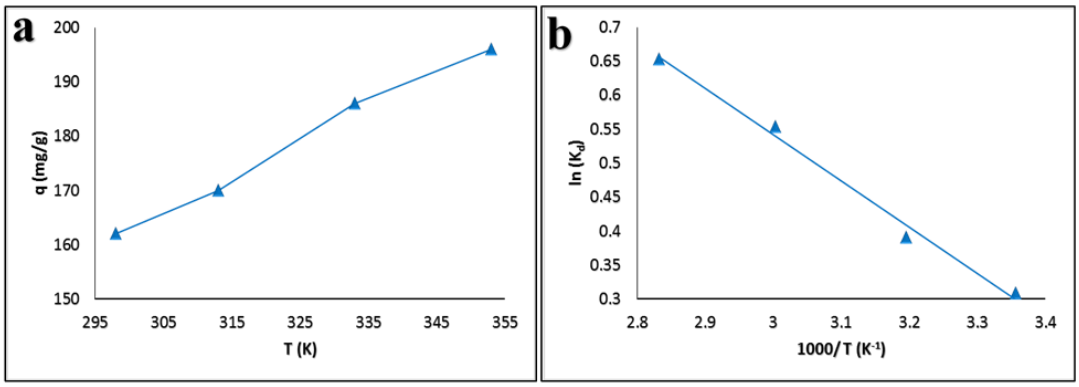

Fig. 6: (a) Effect of temperature on the adsorption capacity of Cd^{2+} ions onto the MZ-A/RGO nanocomposite and (b) adsorption thermodynamic study.

Table 4: Thermodynamic parameters for Cd^{2+} ions adsorption on MZ-A/RGO

Temperature (K)	ΔH^0 (kJ/mol)	ΔS^0 (kJ/mol.K)	ΔG^0 (kJ/mol)
298	5.67	21.50	−0.76
313			−1.02
333			−1.53
353			−1.92

References

1) **Al Zarooni, M. and Abu Al-Rub, F. (2004).** Adsorption of Lead Ions from Aqueous Solution onto Activated Carbon and Chemically-Modified Activated Carbon Prepared from Date Pits. Adsorption Science & Technology - ADSORPT SCI TECHNOL, **22:** 119-134 .
2) **Irshad, M., Shakoor, M., Ali, S., Nawaz, R. and Rizwan, M. (2019).** Synthesis and Application of Titanium Dioxide Nanoparticles for Removal of Cadmium from Wastewater: Kinetic and Equilibrium Study. Water Air and Soil Pollution, **230**(12): 278.
3) **Sun, H., Xia, N., Liu, Z., Kong, F. and Wang, S. (2019).** Removal of copper and cadmium ions from alkaline solutions using chitosan-tannin functional paper materials as adsorbent. Chemosphere, **236**: 124370.
4) **Godt, J., Scheidig, F., Grosse-Siestrup, C., Esche, V., Brandenburg, P., Reich, A. and Groneberg, D. A. (2006).** The toxicity of cadmium and resulting hazards for human health. Journal of occupational medicine and toxicology (London, England), **1**: 22-22.

5) **Trinh, T. T. P. N. X., Quang, D. T., Tu, T. H., Dat, N. M., Linh, V. N. P., Van Cuong, L. and Hieu, N. H. (2019).** Fabrication, characterization, and adsorption capacity for cadmium ions of graphene aerogels. Synthetic Metals, **247:** 116-123.
6) **Sandoval, A., Hernández-Ventura, C. and Klimova, T. E. (2017).** Titanate nanotubes for removal of methylene blue dye by combined adsorption and photocatalysis. Fuel, **198**: 22-30.
7) **Samuel, M. S., Subramaniyan, V., Bhattacharya, J., Chidambaram, R., Qureshi, T. and Pradeep Singh, N. D. (2018).** Ultrasonic-assisted synthesis of graphene oxide – fungal hyphae: An efficient and reclaimable adsorbent for chromium(VI) removal from aqueous solution. Ultrasonics Sonochemistry, **48**: 412-417.
8) **Tiwari, J. N., Mahesh, K., Le, N. H., Kemp, K. C., Timilsina, R., Tiwari, R. N. and Kim, K. S. (2013).** Reduced graphene oxide-based hydrogels for the efficient capture of dye pollutants from aqueous solutions. Carbon, **56**: 173-182.
9) **Chowdhury, S. and Balasubramanian, R. (2014).** Recent advances in the use of graphene-family nanoadsorbents for removal of toxic pollutants from wastewater. Advances in Colloid and Interface Science, **204:** 35-56.
10) **Ji, L., Chen, W., Zhaoyi, x. and Zheng, S. (2013).** Graphene Nanosheets and Graphite Oxide as Promising Adsorbents for Removal of Organic Contaminants from Aqueous Solution. Journal of environmental quality, **42**: 191-198.
11) **Salawudeen, A. O., Tawabini, B. S., Al-Shaibani, A. M. and Saleh, T. A. (2020).** Poly(2-hydroxyethyl methacrylate) grafted graphene oxide for cadmium removal from water with interaction mechanisms. Environmental Nanotechnology, Monitoring & Management, **13:** 100288.
12) **Xu, W., Chen, Y., Zhang, W. and Li, B. (2019).** Fabrication of graphene oxide/bentonite composites with excellent adsorption performances for toluidine blue removal from aqueous solution. Advanced Powder Technology, **30**(3): 493-501.
13) **Hernández-Montoya, V., Pérez-Cruz, M. A., Mendoza-Castillo, D. I., Moreno-Virgen, M. R. and Bonilla-Petriciolet, A. (2013).** Competitive adsorption of dyes and heavy metals on zeolitic structures. Journal of Environmental Management, **116**: 213-221.
14) **Nibou, D., Mekatel, H., Amokrane, S., Barkat, M. and Trari, M. (2010).** Adsorption of Zn2+ ions onto NaA and NaX zeolites: Kinetic, equilibrium and thermodynamic studies. Journal of Hazardous Materials, **173**(1): 637-646.
15) **Liu, J., Huang, Z., Sun, J., Zou, Y. and Gong, B. (2020).** Enhancing the removal performance of Cd(II) from aqueous solutions by NaA zeolite through doped thiourea reduced GO which is trapped within zeolite crystals. Journal of Alloys and Compounds, **815**: 152514.
16) **Sapawe, N., Jalil, A. A., Triwahyono, S., Shah, M. I. A., Jusoh, R., Salleh, N. F. M. and Karim, A. H. (2013).** Cost-effective microwave rapid synthesis of zeolite NaA for removal of methylene blue. Chemical Engineering Journal, **229**: 388-398.
17) **Farghali, M. A., Eldin, T. A. S., Alenizi, A. and Bahnasawy, R. M. E. (2015).** Graphene/ Magnetite Nanocomposite for Potential Environmental Application. International journal of electrochemical science, **10**(1):529-537.
18) **He, K., Chen, G., Zeng, G., Chen, A., Huang, Z., Shi, J. and Hu, L. (2018).** Enhanced removal performance for methylene blue by kaolin with graphene oxide modification. Journal of the Taiwan Institute of Chemical Engineers, **89:** 77-85.
19) **Aouled Mhemed, H., Marin Gallego, M., Largeau, J.-F., Kordoghli, S., Zagrouba, F. and Tazerout, M. (2020).** Gas adsorptive desulfurization of thiophene by spent coffee grounds-derived carbon optimized by response surface methodology: Isotherms and kinetics evaluation. Journal of Environmental Chemical Engineering, **8**(5): 104036.
20) **Iftekhar, S., Ramasamy, D. L., Srivastava, V., Asif, M. B. and Sillanpää, M. (2018).** Understanding the factors affecting the adsorption of Lanthanum using different adsorbents: A critical review. Chemosphere, **204:** 413-430.
21) **Ahmad, S. Z. N., Wan Salleh, W. N., Ismail, A. F., Yusof, N., Mohd Yusop, M. Z. and Aziz, F. (2020).** Adsorptive removal of heavy metal ions using graphene-based nanomaterials: Toxicity, roles of functional groups and mechanisms. Chemosphere, **248:** 126008.
22) **Xu, J., Cao, Z., Zhang, Y., Yuan, Z., Lou, Z., Xu, X. and Wang, X. (2018).** A review of functionalized carbon nanotubes and graphene for heavy metal adsorption from water: Preparation, application, and mechanism. Chemosphere, **195:** 351-364.
23) **Febrianto, J., Kosasih, A. N., Sunarso, J., Ju, Y.-H., Indraswati, N. and Ismadji, S. (2009).** Equilibrium and kinetic studies in adsorption of heavy metals using biosorbent: A summary of recent studies. Journal of Hazardous Materials, **162**(2): 616-645.
24) **Bankole, M. T., Abdulkareem, A. S., Mohammed, I. A., Ochigbo, S. S., Tijani, J. O., Abubakre, O. K. and Roos, W. D. (2019).** Selected Heavy Metals Removal From Electroplating Wastewater by Purified and Polyhydroxylbutyrate Functionalized Carbon Nanotubes Adsorbents. Scientific Reports, **9**(1): 4475.
25) **Al-Ghouti, M. A. and Da'ana, D. A. (2020).** Guidelines for the use and interpretation of adsorption isotherm models: A review. Journal of Hazardous Materials, **393:** 122383.

26) **Mashkoor, F. and Nasar, A. (2020).** Magsorbents: Potential candidates in wastewater treatment technology – A review on the removal of methylene blue dye. Journal of Magnetism and Magnetic Materials, **500**: 166408.

27) **Vijayaraghavan, K., Padmesh, T. V. N., Palanivelu, K. and Velan, M. (2006).** Biosorption of nickel(II) ions onto Sargassum wightii: Application of two-parameter and three-parameter isotherm models. Journal of Hazardous Materials, **133**(1): 304-308.

28) **Kundu, S. and Gupta, A. K. (2006).** Arsenic adsorption onto iron oxide-coated cement (IOCC): Regression analysis of equilibrium data with several isotherm models and their optimization. Chemical Engineering Journal, **122**(1): 93-106.

29) **Weber, T. W. and Chakravorti, R. K. (1974).** Pore and solid diffusion models for fixed bed adsorbers. Aiche Journal, **20:** 228-238.

30) **Farouq, R. and Yousef, N. (2015).** Equilibrium and Kinetics Studies of adsorption of Copper (II) Ions on Natural Biosorbent. International Journal of Chemical Engineering and Applications, **6**(5): 319-324.

31) **A.O, D., Olalekan, A., Olatunya, A. and Dada, A. O. (2012).** Langmuir, Freundlich, Temkin and Dubinin–Radushkevich Isotherms Studies of Equilibrium Sorption of Zn 2+ Unto Phosphoric Acid Modified Rice Husk. J. Appl. Chem., **3**: 38-45.

32) **Araújo, C. S. T., Almeida, I. L. S., Rezende, H. C., Marcionilio, S. M. L. O., Léon, J. J. L. and de Matos, T. N. (2018).** Elucidation of mechanism involved in adsorption of Pb(II) onto lobeira fruit (Solanum lycocarpum) using Langmuir, Freundlich and Temkin isotherms. Microchemical Journal, **137:** 348-354.

33) **Ilyas, A., Muhammad, N., Gilani, M. A., Vankelecom, I. F. J. and Khan, A. L. (2018).** Effect of zeolite surface modification with ionic liquid [APTMS][Ac] on gas separation performance of mixed matrix membranes. Separation and Purification Technology, **205:** 176-183 .

34) **He, P., Wang, W., Du, L., Dong, F., Deng, Y. and Zhang, T. (2012).** Zeolite A functionalized with copper nanoparticles and graphene oxide for simultaneous electrochemical determination of dopamine and ascorbic acid. Analytica Chimica Acta, **739**: 25-30.

35) **Zhao, G., Li, J., Ren, X., Chen, C. and Wang, X. (2011).** Few-Layered Graphene Oxide Nanosheets As Superior Sorbents for Heavy Metal Ion Pollution Management. Environmental Science & Technology, **45**(24): 10454-10462.

36) **Zhang, J., Yang, H., Shen, G., Cheng, P., Zhang, J. and Guo, S. (2010).** Reduction of graphene oxide via L-ascorbic acid. Chem Commun (Camb), **46**(7): 1112-1114.

37) **Moreira, J. C., Santa, R. A. A. B., Nones, J. and Riella, H. G. (2018).** SYNTHESIS OF ZEOLITE 4A FOR OBTAINING ZEOLITE 5A BY IONIC EXCHANGE FOR FULL UTILIZATION OF WASTE FROM PAPER INDUSTRY. Brazilian Journal of Chemical Engineering, **35**: 623-630.

38) **Giroux, M., Sahadeo, E., Libera, R., Maurizi, A., Giles, I. and Marteel-Parrish, A. (2016).** An undergraduate research experience: Synthesis, modification, and comparison of hydrophobicity of zeolites A and X. Polyhedron, **114:** 42-52.

39) **Hu, T., Gao, W., Liu, X., Zhang, Y. and Meng, C. (2017).** Synthesis of zeolites Na-A and Na-X from tablet compressed and calcinated coal fly ash. Royal Society Open Science, **4**: 170921.

40) **Li, S., Lu, X., Xue, Y., Lei, J., Zheng, T. and Wang, C. (2012).** Fabrication of Polypyrrole/Graphene Oxide Composite Nanosheets and Their Applications for Cr(VI) Removal in Aqueous Solution. PLOS ONE, **7**(8), e43328.

41) **Sanaeepur, H., Kargari, A. and Nasernejad, B. (2014).** Aminosilane-functionalization of a nanoporous Y-type zeolite for application in a cellulose acetate based mixed matrix membrane for CO2 separation. RSC Advances, **4**(109): 63966-63976.

42) **Suddai, A., Nuengmatcha, P., Sricharoen, P., Limchoowong, N. and Chanthai, S. (2018).** Feasibility of hard acid–base affinity for the pronounced adsorption capacity of manganese(ii) using amino-functionalized graphene oxide. RSC Advances, **8**(8): 4162-4171.

43) **Wang, C., Leng, S., Xu, Y., Tian, Q., Zhang, X., Cao, L. and Huang, J.-F. (2018).** Preparation of Amino Functionalized Hydrophobic Zeolite and Its Adsorption Properties for Chromate and Naphthalene. Minerals, **8**: 145.

44) **Huang, T., Yan, M., He, K., Huang, Z., Zeng, G., Chen, A. and Chen, G. (2019).** Efficient removal of methylene blue from aqueous solutions using magnetic graphene oxide modified zeolite. Journal of Colloid and Interface Science, **543**: 43-51.

45) **Musyoka, N., Petrik, L., Hums, E., Kuhnt, A. and Schwieger, W. (2013).** Thermal stability studies of zeolites A and X synthesized from South African coal fly ash. Research on Chemical Intermediates, **41**: 575–582.

46) **Motsi, T., Rowson, N. A. and Simmons, M. J. H. (2011).** Kinetic studies of the removal of heavy metals from acid mine drainage by natural zeolite. International Journal of Mineral Processing, **101**(1): 42-49.

47) **Shavandi, M. A., Haddadian, Z., Ismail, M. H. S., Abdullah, N. and Abidin, Z. Z. (2012).** Removal of Fe(III), Mn(II) and Zn(II) from palm oil mill effluent (POME) by natural zeolite. Journal of the Taiwan Institute of Chemical Engineers, **43**(5): 750-759.

48) **Anitha, T., Kumar, P. S., Kumar, K. S., Ramkumar, B. and Ramalingam, S. (2015).** Adsorptive removal of Pb(II) ions from polluted water by newly synthesized chitosan–polyacrylonitrile blend: Equilibrium, kinetic, mechanism and thermodynamic approach. Process Safety and Environmental Protection, **98**: 187-197 .

49) **Aksu, Z. and Tezer, S. (2005).** Biosorption of reactive dyes on the green alga Chlorella vulgaris. Process Biochemistry, **40**(3): 1347-1361.

50) **Langmuir, I. (1918).** THE ADSORPTION OF GASES ON PLANE SURFACES OF GLASS, MICA AND PLATINUM. Journal of the American Chemical Society, **40**(9): 1361-1403.

51) **Narvekar, A. A., Fernandes, J. B. and Tilve, S. G. (2018).** Adsorption behavior of methylene blue on glycerol based carbon materials. Journal of Environmental Chemical Engineering, **6**(2): 1714-1725.

52) **Nitzsche, R., Gröngröft, A. and Kraume, M. (2019).** Separation of lignin from beech wood hydrolysate using polymeric resins and zeolites – Determination and application of adsorption isotherms. Separation and Purification Technology, **209**: 491-502.

53) **Ding, Z., Hu, X., Zimmerman, A. R. and Gao, B. (2014).** Sorption and cosorption of lead (II) and methylene blue on chemically modified biomass. Bioresource Technology, **167:** 569-573.

54) **Wang, M., Cai, H. and Zhang, J. J. C. E. T. (2018).** Application Research on the Adsorption of Cadmium Ion in Wastewater by Zeolite Molecular Sieve. CHEMICAL ENGINEERING TRANSACTIONS, **71**: 403-408.

55) **Liu, J., Huang, Z., Sun, J., Zou, Y., Gong, B. J. J. o. A. and Compounds. (2020).** Enhancing the removal performance of Cd (II) from aqueous solutions by NaA zeolite through doped thiourea reduced GO which is trapped within zeolite crystals. **815:** 152514.

56) **Vilela, P. B., Matias, C. A., Dalalibera, A., Becegato, V. A. and Paulino, A. T. (2019).** Polyacrylic acid-based and chitosan-based hydrogels for adsorption of cadmium: Equilibrium isotherm, kinetic and thermodynamic studies. Journal of Environmental Chemical Engineering, **7**(5): 103327.

57) **Wu, S., Zhang, K., Wang, X., Jia, Y., Sun, B., Luo, T. and Liu, J. (2015).** Enhanced adsorption of cadmium ions by 3D sulfonated reduced graphene oxide. Chemical Engineering Journal, **262:** 1292-1302.

58) **Kong, X., Huang, G., Han, Z., Xu, Y., Zhu, M. and Zhang, Z. (2017).** Evaluation of zeolite-supported microscale zero-valent iron as a potential adsorbent for Cd2+ and Pb2+ removal in permeable reactive barriers. Environmental Science and Pollution Research, 24: 1-8.

59) **Madala, S., Nadavala, S. K., Vudagandla, S., Boddu, V. M. and Abburi, K. (2017).** Equilibrium, kinetics and thermodynamics of Cadmium (II) biosorption on to composite chitosan biosorbent. Arabian Journal of Chemistry, **10:** S1883-S1893.

60) **Zhou, G., Liu, C., Tang, Y., Luo, S., Zeng, Z., Liu, Y. and Chu, L. (2015).** Sponge-like polysiloxane-graphene oxide gel as a highly efficient and renewable adsorbent for lead and cadmium metals removal from wastewater. Chemical Engineering Journal, **280:** 275-282.

61) **Ozay, O., Ekici, S., Baran, Y., Aktas, N. and Sahiner, N. (2009).** Removal of toxic metal ions with magnetic hydrogels. Water Research, **43**(17): 4403-4411.

62) **Veneu, D., Schneider, C., Monte, M., Cunha, O. and Yokoyama, L. (2017).** Cadmium Removal by Bioclastic Granules (Lithothamnium calcareum): Batch and Fixed-Bed Column Systems Sorption Studies. Environmental Technology, **39**: 1-43.

63) **Samuel, M. S., Selvarajan, E., Subramaniam, K., Mathimani, T., Seethappan, S. and Pugazhendhi, A. (2020).** Synthesized β-cyclodextrin modified graphene oxide (β-CD-GO) composite for adsorption of cadmium and their toxicity profile in cervical cancer (HeLa) cell lines. Process Biochemistry, **93**: 28-35.

64) **Khan, Z. H., Gao, M., Qiu, W., Islam, M. S. and Song, Z. (2020).** Mechanisms for cadmium adsorption by magnetic biochar composites in an aqueous solution. Chemosphere, **246**: 125701.

65) **Luo, C., Wei, R., Guo, D., Zhang, S. and Yan, S. (2013).** Adsorption behavior of MnO2 functionalized multi-walled carbon nanotubes for the removal of cadmium from aqueous solutions. Chemical Engineering Journal, **225**: 406-415.

66) **Subbaiah, M. V. and Kim, D.-S. (2016).** Adsorption of methyl orange from aqueous solution by aminated pumpkin seed powder: Kinetics, isotherms, and thermodynamic studies. Ecotoxicology and Environmental Safety, **128**: 109-117.

67) **Gusain, D., Singh, P. K. and Sharma, Y. C. (2016).** Kinetic and equilibrium modelling of adsorption of cadmium on nano crystalline zirconia using response surface methodology. Environmental Nanotechnology, Monitoring & Management, **6**: 99-107.

68) **Kołodyńska, D., Hałas, P., Franus, M. and Hubicki, Z. (2017).** Zeolite properties improvement by chitosan modification—Sorption studies. Journal of Industrial and Engineering Chemistry, **52**: 187-196.